Molecular Crystals and Liquid Crystals
Publication details, including instructions for authors and subscription information:
http://www.tandfonline.com/loi/gmcl20

Liquid Crystal Based Polarization Gratings for Spectro-Polarimetric Applications

E. Lepera [a], C. Provenzano [a], P. Pagliusi [a b] & G. Cipparrone [a b]
[a] Department of Physics, University of Calabria, Ponte P. Bucci Cubo 33B, Rende (CS), 87036, Italy
[b] CNR-IPCF, UOS Cosenza, and Excellence Centre CEMIF.CAL, Ponte P. Bucci, Rende (CS), 87036, Italy
Version of record first published: 18 Apr 2012.

To cite this article: E. Lepera , C. Provenzano , P. Pagliusi & G. Cipparrone (2012): Liquid Crystal Based Polarization Gratings for Spectro-Polarimetric Applications, Molecular Crystals and Liquid Crystals, 558:1, 109-119

To link to this article: http://dx.doi.org/10.1080/15421406.2011.653716

Mol. Cryst. Liq. Cryst., Vol. 558: pp. 109–119, 2012

ISSN: 1542-1406 print/1563-5287 online
DOI: 10.1080/15421406.2011.653716

Taylor & Francis
Taylor & Francis Group

Liquid Crystal Based Polarization Gratings for Spectro-Polarimetric Applications

E. LEPERA,[1,*] C. PROVENZANO,[1] P. PAGLIUSI,[1,2] AND G. CIPPARRONE[1,2]

[1]Department of Physics, University of Calabria, Ponte P. Bucci, Cubo 33B, Rende (CS), 87036, Italy
[2]CNR-IPCF, UOS Cosenza, and Excellence Centre CEMIF.CAL, Ponte P. Bucci, Rende (CS), 87036, Italy

Two approaches to produce near-ideal Cycloidal Optical Axis Gratings (OAGs) based on liquid crystalline materials have been proposed. Both methods rely on polarization holograms recorded on the photoaligning substrates for liquid crystal devices. In the first case, a nematic LC layer, made of low molar mass mesogens, is confined between two parallel substrates, both imposing spatially periodic planar alignment. In the second case, a reactive mesogen (RM) is coated on a single aligning substrate. The unique polarization properties of the OAG have been exploited for the development of a photopolarimeter and a real time and artifact-free circular dichroism spectrograph.

Keywords Cycloidal optical axis grating; polarization holography; polarimetry

Introduction

Cycloidal Optical Axis Gratings (OAGs) are an important kind of polarization gratings and can be defined broadly as diffraction gratings with a spatially varying birefringent and/or dichroism. While many unique properties have been theoretically identified and compelling applications studied [1, 2] their practical use has been severely limited due to the difficulties in producing cycloidal OAG with optimal performances, such as high polarization contrast and diffraction efficiency, small spatial period, low scattering, chemical, optical and thermal stability. Substantial efforts have been devoted to investigate liquid crystal (LC) gratings obtained through control over the local surface anchoring and several procedures have been proposed to achieve in-plane spatially periodic orientation of the nematic director, such as photolithography [3], laser scanning [4], mask photopolymerization [5] and stylus patterning [6]. Unfortunately, all of them suffer of intrinsic drawbacks, mainly because they are limited to discrete-step patterns, which end up in optical axis gratings with inadequate performances. We focus in this work on two viable approaches to produce near-ideal Cycloidal Optical Axis Gratings (OAGs), both based on polarization holography and nematic LC amplification of the optical anisotropy of thin photoaligning layers. In the first case, the nematic LC layer, made of low molar mass mesogens, is confined between two parallel substrates, both imposing spatially periodic planar alignment. In the second case, a reactive mesogen

*Address correspondence to E. Lepera, Department of Physics, University of Calabria, Ponte P. Bucci, Cubo 33B, Rende (CS), 87036, Italy. E-mail: eugenia.lepera@fis.unical.it

(RM) is coated on a single aligning substrate and then photo-polymerized to permanently harden the periodic anisotropic structure. Moreover, the ability of cycloidal optical axis gratings (OAGs) to fully transfer the energy of an unpolarized incident light beam into the ± 1st diffraction orders is explored below for the realization of a photopolarimeter and for the development of a real time and artifact-free CD spectroscopy.

Cycloidal Optical Axis Gratings

The OAG is made of a slab of linear birefringence (and/or dichroic) material whose in-plane optical axis continuously varies with position along the grating vector direction, as shown in Fig. 1(a) [7, 8]. Generally, there are three beams at the output of cycloidal OAGs: the transmitted (0th order diffraction) and the ±1st order diffracted beams. When a light beam with generic polarization impinges on the OAG, the ±1-orders are always orthogonally circularly polarized and their intensities are proportional to the right-handed (RCP) and left-handed (LCP) circularly polarized light component of the incident beam [7–10]. The diffraction efficiency for the total of the ±1st diffracted orders ($\eta_{\pm 1}$) for unpolarized incident light is determined by the following formula for an ideal grating with no absorption or losses:

$$\eta_{+1} + \eta_{-1} = \sin^2(\pi d \Delta n/\lambda) \tag{1}$$

Here d is the grating thickness and Δn is the optical anisotropy at the wavelength λ. It is worth noting here that the cumulative diffraction efficiency of the cycloidal OAG does not depend on the polarization state of the impinging beam and reaches 100% at those wavelengths for which the half-wave plate condition is fulfilled (i.e. $d\Delta n = m\lambda/2$ where m is an odd integer). According to Eq. (1), it is possible to obtain high diffraction efficiency for almost any desired wavelength and in a broad spectral range, by varying the optical retardation $d\Delta n$ (i.e. changing the thickness and/or the birefringence of the material).

Beside the potential of 100% diffraction efficiency [11] into the ±1-orders and the relatively wide diffraction bandwidth [12] of the cycloidal OAG, its most interesting feature for the future applications (i.e. flat panel displays, sensor, telecommunication, and storage applications) is the strong polarization sensitive diffraction.

The most straightforward approach to fabricate practical OAGs with high efficiency, low optical scattering, and robust stability for the entire visible and near-infrared wavelengths relies on polarization holography, with organic materials containing azobenzene

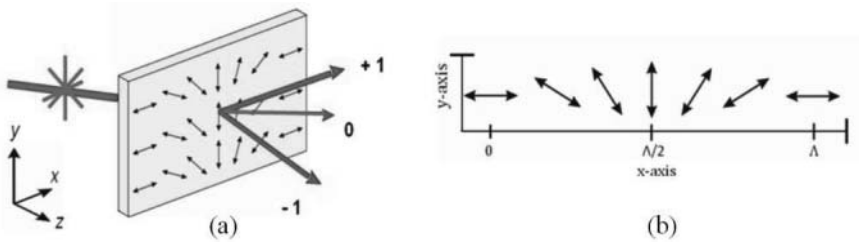

Figure 1. (a) Cycloidal optical axis grating (OAG), in which the local optical axis lies in the plane of the film (xy-plane) and uniformly rotates along the x-axis. (b) Illustration of polarization pattern created by orthogonal circularly-polarized beams.

moieties, and polarization sensitive anisotropic materials [7, 8]. Holographic OAGs are generally recorded with orthogonal linear or orthogonal circular polarized beams to ensure spatial homogeneity of the light intensity distribution. In particular, a constant intensity, rectilinear light vibrations, with spatially varying orientation, is obtained from superposition of two orthogonal circularly polarized waves propagating, in slightly different directions. If a polarization sensitive photoaligning layer is exposed to the interference optical field, a polarization hologram is produced via photoinduced anisotropy, whose local axis is correlated to the corresponding polarization direction. The optical axis orientation in these gratings, shown below in Fig. 1(b) undergoes a continuous and complete in-plane rotation along the grating vector, according to the spatial profile $n(x) = [\cos(\pi x/\Lambda), \sin(\pi x/\Lambda), 0]$ where Λ is the grating period because $n(x)$ and $-n(x)$ are physically identical. Such a patterned layer can work as a template for the adjacent nematic LC slab, by providing the necessary anchoring energy to orient the nematic director parallel to the local easy-axis [13, 14]. Thus, the LC layer behaves as a replica of the polarization hologram recorded on the photosensitive layer. The control of the thickness d and the birefringence Δn of the nematic LC layer allows for tuning diffraction efficiency curves according to the spectral range of interest, still keeping the grating thickness small enough (i.e. $\sim$1 μm) to reduce light absorption and scattering.

Fabrication of Cycloidal OAGs

Here we discuss on two viable approaches to produce near-ideal cycloidal OAGs, both share the same photoaligning azobenzene material and deposition procedure [15, 16], which enable to obtain high quality thin (i.e. less than 10nm-thick) command layers, characterized by fairly high azimuthal anchoring energy (i.e. 10^{-4} J/m^2, comparable to rubbed polyimide). The dichroic azobenzene dye we use belongs to the class of sulphuric bis-azobenzene dyes which are drawing interest as photoaligning agent for low-molecular-weight LCs, polymeric and polymerizable LCs, because of their photosensitivity, high thermal, photochemical and electrochemical stability. When irradiated with linearly polarized light within its spectral sensitivity range (which extends up to 500 nm), the dye provides LC planar alignment perpendicular to the light polarization, via anisotropic van der Waals interaction between the partially and strongly conjugated LC and dye molecules, respectively [15].

The dye is dissolved in N-N-dimethylformamide at concentration of 1% by weight. The solution is filtered to 0.22 μm and spin coated (FR10KPA, CaLCTec S.r.l) on glass substrates at 800 rpm for 10s then at 3000 rpm for 60s. The substrates were cleaned in an ultrasonic bath of NaOH in water (5% by weight) at 40°C for 10 minutes and then in a plasma cleaner for 10 minutes to remove organic contamination, immediately before coating the dye layer. The dye films are dried at 100°C for 30 minutes, to let the solvent evaporate and to promote the adhesion of the dye molecules to the glass substrates. The polarization pattern is produced by the interference of two Ar^+ laser beams ($\lambda = 458$ nm) with opposite circular polarizations and identical intensity $\sim$15 mW/cm^2. The polarization holograms are obtained exposing the dye-coated substrates to the interference optical field for 2 minutes. In order to fulfill the stability condition for a perfect bulk replica of the director distribution imposed by the surfaces (typically $d/2\Lambda < 0.3$) [17], the spatial periodicity Δ of the optical axis pattern has been chosen equal to 8 μm, so that it is much larger than the typical thickness $d \approx 0.7 \div 3$ μm of the LC layer.

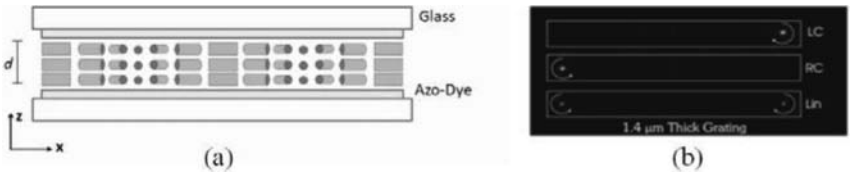

Figure 2. (a) Scheme of the LC OAG confined between two dye-coated glass substrates. The polarization holograms are recorded on both the photoaligning layers and then the LC is infiltrated. The nematic director follows the directions imposed by the two substrates throughout the cell thickness. Two grating periods are shown. (b) Diffraction of He-Ne beam into the ± 1 orders only.

Liquid Crystal OAGs

In the first approach, two substrates are used to assemble a cell of proper thickness in a clean-room environment (Class 100). The empty cell, with the dye-coated surfaces facing each other, is exposed to the polarization pattern in order to record two registered polarization holograms on the two photosensitive aligning layers. The cell is filled by capillary action with an eutectic nematic LC mixture E7 ($\Delta n = 0.23$ at $\lambda = 589$ nm) above the clearing temperature (at 65°C) and slowly cooled to the nematic phase, down to room temperature (Fig. 2(a)). The resulting LC OAGs show excellent optical and diffraction properties, such as low scattering, high contrast ratio and polarization selectivity. Close to 100% diffraction efficiency into the ± 1-orders can be obtained controlling the cell thickness d and/or adjusting the effective birefringence Δn by temperature or by reorienting the nematic director with an external electric field [18]. Circularly polarized light beam impinging on the LC OAG produced with this method is diffracted into a single order ($+1$ or -1, depending on the helicity) with a large contrast ratio (i.e., typically $\eta_{+1}/\eta_{-1} \approx 2000$ Fig. 2(b)). Linearly polarized light beam is uniformly diffracted into the ± 1-orders (i.e., typically $\eta_{+1} - \eta_{-1}|/(\eta_{+1} + \eta_{-1}) \approx 10^{-3}$), which exhibit almost ideal opposite circular polarizations, as demonstrated below by the following analyses.

Reactive Nematic Mesogen OAGs

In the second approach, a single photoaligning substrate is exposed to the interference field and, afterward, it is coated by a solution of reactive nematic mesogens (RM) [12–14, 19, 20]. The RM film can be fully polymerized to achieve OAGs with enhanced optical and mechanical stability. Here we report the results obtained by using a commercial RM mixture (30% by weight) in propylene glycol monomethyl ether acetate (RMS03-001C by Merck KGaA, $n_0 = 1.529$ and $\Delta n = 0.155$ @ 589 nm, 20°C). The RM solution is spin-coated on the previously patterned aligning substrate at 3000 rpm for 30 s.

The coated substrate is baked on a hot-plate at 55°C for 60s to let the residual solvent evaporate and to favor the alignment of the uncured RM layer. The latter is then photo-polymerized under nitrogen atmosphere by exposing it to the unpolarized UV light of a fluorescent lamp ($\lambda_{max} = 365$ nm, intensity ~ 0.1 mW/cm^2) for 2 hours (Fig. 3(a). All the processes, beside the polarization hologram recording, are carried out in clean-room environment (Class 100). The microscope images of the RM OAG between crossed polarizers (Fig. 3(b)) show a neat optical modulation. The resulting polymeric RM OAG has an average thickness of $d \sim 1$ μm and exhibits a long-range variation within 5% over a fairly large area (several cm^2). Moreover, it is easier to control the mean film thickness either by changing the concentration of solid content in the RM solution, by adjusting the

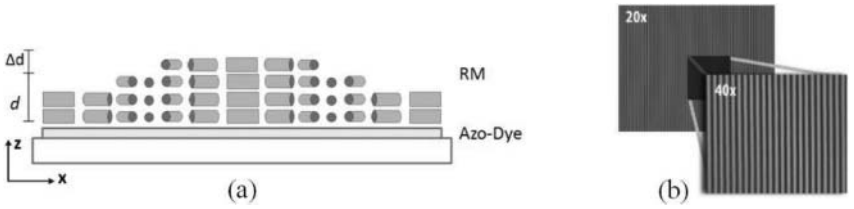

Figure 3. (a) Scheme of the RM OAG. The RM mixture is spin-coated on a single photoaligning substrate. According to the analyses, the nematic director follows the direction imposed by the aligning layer throughout the RM film thickness. Nevertheless a surface relief grating is superimposed to the optical axis modulation. Two grating periods are shown. (b) Optical microscope image of the RM OAG between two crossed polarizers (parallel to the x- and y-axis, respectively) with different magnifications of the objective: 20×, 40×.

rotational speed or even by stacking multiple RM layers. On the other hand, first attempts to fabricate RM OAGs according to this approach have produced gratings with inadequate optical properties, as demonstrated by the following analyses of the polarization state and the diffraction behavior of the ±1-orders.

Characterization of Grating Diffraction

A linearly polarized He-Ne laser ($\lambda = 633$ nm) is used as probe beam in order to investigate the polarization state of the diffracted beams. In Fig. 4, polarization analysis of the three diffracted beams (0-order and the ±1-orders beams) of the LC OAG for a p-polarized probe beam are reported. The normalized intensity of the 0- and ±1-orders are measured after a linear polarizer, versus the angle of its transmission axis. For both the ±1-orders the intensity after the polarizer is nearly constant (standard deviation ∼0.01), indicative of excellent circular polarization. The 0-order preserves the linear polarization state of the incident beam. Unfortunately, the LC OAGs produced according to this method still have few important weaknesses such as the inaccurate control of the grating thickness in the 1 μm range and the reduced optical stability of the aligning surfaces. Moreover, the polarization hologram recorded in the photo-aligning dye layer, and hence the OAG in the nematic LC layer, has weak optical stability, as it can be erased by the continuous exposure to the UV-Vis light of the high-intensity lamp. Such a major drawback could be

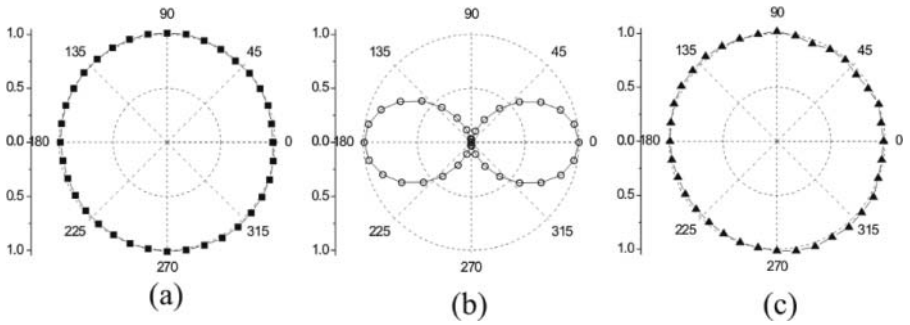

Figure 4. Polar plots of the normalized intensity of the +1 (a), 0 (b) and −1 (c) diffracted beams after a linear polarizer versus the angle of the polarizer axis.

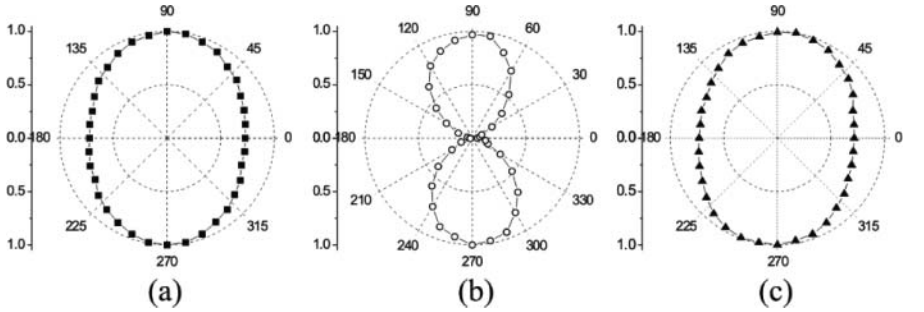

Figure 5. Polar plots of the normalized intensity of the +1 (a), 0 (b) and −1 (c) diffracted beams after a linear polarizer versus the angle of the polarizer axis. It is evident that both ±1-orders are not circularly polarized.

overcome either by stabilizing the photoaligning layer right after the polarization hologram has been recorded (i.e., limiting the rotational mobility of dye molecules by mixing them with a cross-linkable polymer) or by hardening the nematic LC director configuration itself (i.e., adopting a polymer-stabilized liquid crystal structure).

In Fig. 5, polarization analysis of the three diffracted beams (0-order and the ±1-orders beams) of the RM OAG for a s-polarized probe beam are reported. The normalized intensity of the ±1-orders beams after a linear polarizer changes significantly versus the angle of the polarizer axis, signifying that the ±1-orders are not circularly polarized, as they should be in case of an ideal Cycloidal OAG. Furthermore, removing the polarizer on the diffracted beams path and using a half-wave plate to rotate the polarization plane of the linearly polarized He-Ne probe beam, the ±1-orders diffraction efficiency of RM OAG is measured versus the azimuthal angle α of the linearly polarized light. In Fig. 6 we report the diffraction efficiency of the +1-order versus the angle α over a 2π-range.

Also in this case, the data make evidence of a significant deviation from the theoretical behavior of a pure OAG, according to which the diffraction efficiency of the ±1-orders does not depend on the angle of polarization. In this respect, it is known that recording of

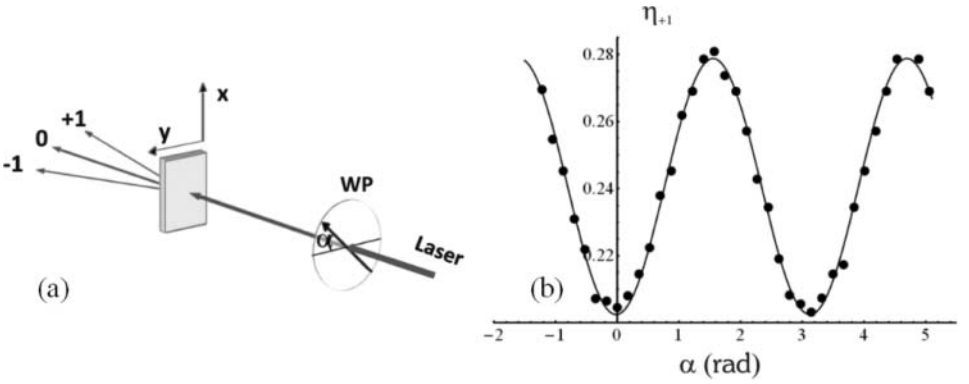

Figure 6. (a) Measurement setup including waveplates (WP) and the RM OAG. (b) Diffraction efficiency of the RM OAG at the +1-order (black dots, •) is measured versus the azimuthal angle α the polarization plane of the incident He-Ne beam forms with the x-axis ($\alpha = 0$ and $\pi/2$ for p- and s-polarized incident beam, respectively). Solid line is the fit of the experimental data using the function of Eq. (6).

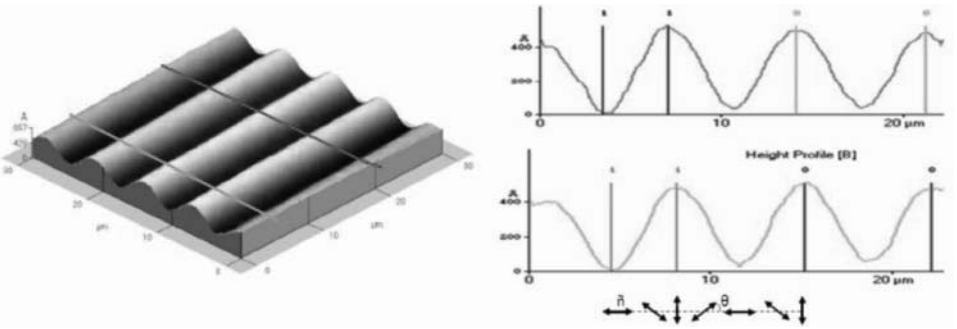

Figure 7. Topography of the RM OAG measured by AFM shows periodic relieves with a peak-to-valley depth ∼50 nm and the same spatial periodicity of the optical axis grating (∼8 μm).

polarization gratings in anisotropic media is often associated with the formation of surface relief gratings (SRG), which may significantly affect the diffraction properties of the former ones [21, 22]. While the occurrence of SRGs is hindered in the first approach, since the OAGs are confined between two solid substrates, they are possible in this second approach at the air-RM interface. Indeed, investigation of the RM film topography via atomic force microscopy (AFM) shows an undulation of the free surface characterized by the same periodicity of the OAG and a peak-to-valley depth of ∼50 nm (see Fig. 7).

A simple theoretical model based on Jones calculus is considered here to verify if the sole periodic modulation of the surface topography is enough to explain the diffraction properties of the RM grating. The model takes into account both the OAG and the SRG, which is regarded as a sinusoidal correction to the polymer film thickness

$$d + \Delta d \, \cos(qx + \delta_0) \tag{2}$$

where Δd is the modulation amplitude (half of the relief depth) and δ_0 the spatial phase shift of the SRG with respect to the OAG $n(x) = [\cos(\pi x/\Lambda),\ \sin(\pi x/\Lambda), 0]$. The Jones transmission matrix of the SRG is [21]

$$J^{SRG} = \begin{pmatrix} \exp[i\,\Delta\psi\,\cos(qx + \delta_0)] & 0 \\ 0 & \exp[i\,\Delta\psi\,\cos(qx + \delta_0)] \end{pmatrix} \tag{3}$$

where $\Delta\psi = 2\pi\,\Delta d(n_p - n_a)/\lambda$ is half of the phase shift due to the surface relief, n_p and n_a are the refractive index of the polymer (i.e., average value between n_o and $n_e = n_o + \Delta n$) and of the adjacent medium (i.e., $n_a \approx 1$ for air), respectively. The diffracted fields can be evaluated multiplying the incident linearly polarized field by the total transmission matrix

$$E_{OUT} = J^{SRG}\,J^{OAG}\,E_{IN} = J^{SRG}\,J^{OAG} \begin{pmatrix} \cos\alpha \\ \sin\alpha \end{pmatrix} \tag{4}$$

and then decomposing the total Jones matrix $J^{SRG}\,J^{OAG}$ into the contributions of the different orders of diffraction, exploiting the following expansion in Bessel functions of the first kind.

$$e^{i\,\Delta\psi\,\cos(qx + \delta_0)} = J_0(\Delta\psi) + \sum_{m=1}^{\infty} i^m J_m(\Delta\psi) \left[e^{im\cos(qx+\delta_0)+e} - im\cos(qx + \delta_0) \right] \tag{5}$$

Limiting the analysis to the ±1-orders and adopting the approximation $J_0(\Delta\psi) \approx 1$, $J_1(\Delta\psi) \approx \Delta\psi/2$ and $J_2(\Delta\psi) \approx 0$, we can fit the data reported in Fig. 6 considering the following function

$$n_{\pm1}(\alpha) = \frac{1}{8}[2 + \Delta\psi^2 + (\Delta\psi^2 - 2)\cos(2\Delta\phi) + 2\Delta\psi \sin(2\Delta\phi)\cos(\delta_0 + 2\alpha)] \quad (6)$$

for the values of the parameters $\Delta\phi \approx 0.77$, $\Delta\psi \approx 0.15$ and $\delta_0 \approx \pi$. The value of spatial phase shift means that the peaks of the SRG correspond to the regions in which the optical axis is oriented orthogonally to the grating vector (i.e., $n(x) = [0, 1, 0]$ along the fringes, see Fig. 3). Assuming $\Delta n = 0.155$, $n_p = 1.6$ and $n_a = 1$ we calculate the average film thickness $d \approx 1.0$ μm and the relief modulation amplitude $\Delta d \approx 25$ nm (i.e. peak-to-valley relief depth ≈50 nm), which are both in excellent agreement with the AFM measurements. These results confirm the adequacy of the simple theoretical model discussed here to interpret the optical diffraction properties of the RM OAG, and suggest that the discrepancy versus the ideal cycloidal OAG is merely due to the superimposed SRG. In this respect, we are exploring few strategies to overcome the disadvantage of the SRG for the optical properties of the grating by managing the air-RM interface, both with surfactants, aimed at enforcing in-plane orientation of the nematic director at the free RM surface, and with an overlaid planarizing coating made of photoreactive isotropic monomers, aimed at transferring a planar topography on the underlying RM grating. An ongoing work in our laboratory is based on the use of the nematic RM infiltrated between two aligning solid substrates and then photo-polymerized, in order to guarantee the mechanical and optical stability of the polymeric OAG and simultaneously avoid the formation of the SRG, thus taking advantage of both the described approaches.

Applications

The stability of the recorded gratings and the high induced birefringence of the material, open up the possibility of interesting applications of the gratings to different optical devices. Current tecnologies use several optical and electro-optical elements, different absorbing polarizers, dispersive elements (prism or gratings), phase modulator, which make them very inefficient because of its intrinsic limitations in real-time and artifact-free measurements.

Potential application of these cycloidal OAGs is envisioned in the field of polarimetry, in particular, a new type of photopolarimeter based on two different kinds of diffraction gratings (two-grating photopolarimeter) for simultaneous measurements of the Stokes parameters has been realized [23]. The main component of the instrument is a LC OAG prepared as reported previously. The second fundamental element is a conventional transmission grating recorded by means of an intensity holographic technique in a thin film of a photopolymer. The two gratings constitute the main elements of the device, which also includes two fixed polarizers and four detectors (photodiodes). A scheme of the two-grating photopolarimeter (TGP) is shown in Fig. 8(a).

The light beam to be measured (I_0) impinges onto the polarization grating (PG), and the first diffracted beams I_{-1} (I_1) and I_{+1} (I_2) are detected by the photodiodes Ph_1 and Ph_2, respectively. Furthermore, the transmitted beam is diffracted again by an intensity grating (IG) in which the first orders (I_3 and I_4) are collected by the photodiodes Ph_3 and Ph_4, after passing through polarizers P_{45° and P_{0°.

The four output signals (i_i) are sent to an analog to-digital circuit board of a PC that controls the experiment.

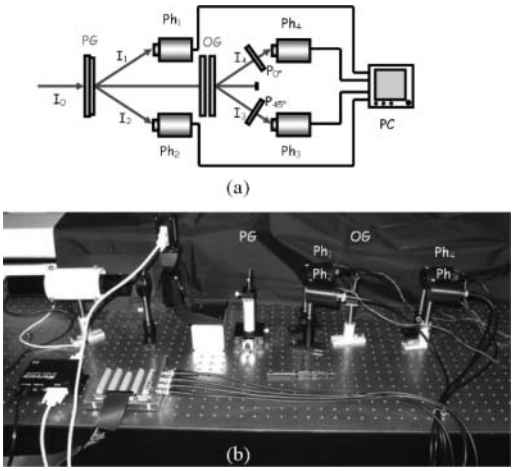

Figure 8. (a) Scheme of the TGP. I_0, incident beams; I_1–I_4, diffracted beams; PG, polarization grating; IG, intensity grating; $P_{0°}$ and $P_{45°}$, polarizers; Ph_1–Ph_4, photodiodes; PC, personal computer with acquisition system. (b) Picture of TGP.

This photopolarimeter has an extreme simplicity of tuning, is free of modulating or moving parts, is easy to calibrate, and it can operate over the whole visible spectral range. Only detector speed and electronics acquisition processes limit the rate at which data can be taken by the instrument; hence it can be useful in real-time measurements.

Moreover, the polarization sensitive diffraction of the cycloidal OAGs suggested an original approach for real-time and artifact-free CD spectroscopy [25]. The central optical element of the proposed CD spectrograph is again a single polarizing optical element (i.e., no wave plates or polarizers; no moving or modulating elements, as photoelastic modulators; no lock-in amplifiers which slow down the CD spectral aquisition) that radically reduces the

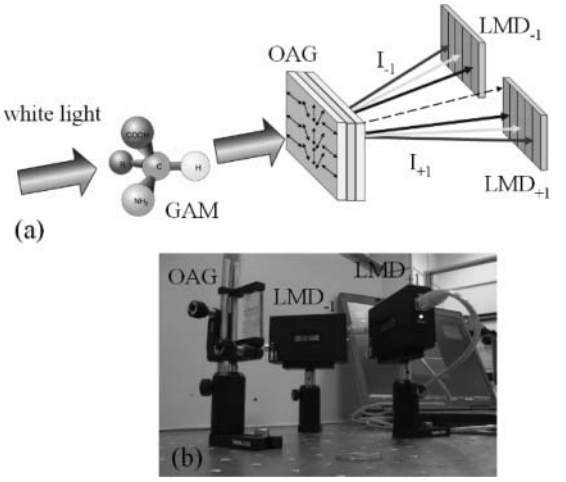

Figure 9. (a) Scheme illustrating the operation principle of the method for diffractive CD spectroscopy. White unpolarized light is collimated on the sample (i.e. a general anisotropic medium, GAM) and its transmission portion is directed to the OAG. The intensities of ±1-orders are measured at each wavelength via linear multi-channel detectors (LMD). (b) Picture of CD spectrograph.

sources of instrumental artifacts [24, 25]. The working principle of the proposed method for CD spectroscopy is illustrated in Fig. 9(a), where a simplified scheme of the diffractive CD spectrograph is reported. The broad-bandwidth (i.e., white) unpolarized light emitted by a high intensity source is collimated and directed to the sample without further bandwidth or polarization adjustment. The light transmitted by the sample impinges on the Cycloidal OAG, which in turn diffracts the light into the zero-order (0) and the two first-order (± 1) beams. The different spectral components of the beams diffracted into the ± 1-orders are angularly dispersed, and the wavelength-dependent intensities are simultaneously measured by linear multi-channel detectors (LMD). The CD spectrum of the sample is then evaluated starting from the intensity of the ± 1-orders at each wavelength [24, 25].

Conclusions

Two fabrication strategies aimed to achieve cycloidal OAGs with optimal performances have been described and their advantage and downsides discussed. In particular, polarization holography, based on the interference of two orthogonal circular polarized beams, and photo-anisotropic aligning material have been exploited to produce cycloidal OAG in birefringent nematic layers. The latter perform as replicas of the faint polarization hologram recorded in the thin photosensitive aligning film. The cases of low molar mass nematic LC sandwiched in a planar cell and of photo-reactive mesogenic monomers spincasted on top of the aligning substrate have been studied experimentally and the results interpreted with a simple model. The LC gratings confined between substrates have demonstrated excellent optical quality, resembling ideal cycloidal OAG. The RM gratings are less prone to optical degradation, thus exhibiting higher optical and mechanical stability, but are affected by detrimental periodic undulation of the free surface. Two polarimetric applications of the OAG have been reported.

References

[1] Gori, F. (1999). *Opt. Lett.*, *24*, 584.
[2] Bomzon, Z., Biener, G., Kleiner, V., & Hasman, E. (2001). *Opt. Lett.*, *26*, 1711.
[3] Chen, J., Bos, P. J., Vithana, H., & Johnson, D. L. (1995). *App. Phys. Lett.*, *67*, 2588–2590.
[4] Gibbons, W. M., & Sun, S. T. (1994). *Appl. Phys. Lett.*, *65*, 2542–2544.
[5] Zhou, J., Collard, D. M., & Srinivasarao, M. (2006). *Opt. Lett.*, *31*, 652–654.
[6] Wen, B., Petschek, R. G., & Rosenblatt, C. (2002). *Appl. Opt.*, *41*, 1246–1250.
[7] Nikolova, L., & Todorov, T. (1984). *Opt. Acta*, *31*, 579–588.
[8] Tervo, J., & Turunen, J. (2000). *Opt. Lett.*, *25*, 785–786.
[9] Gori, F. (1999). *Opt. Lett.*, *24*, 584–586.
[10] Cipparrone, G., Mazzulla, A., Palto, S. P., Yudin, S. G., & Blinov, L. M. (2000). *Appl. Phys. Lett.*, *77*, 2106–2108.
[11] Provenzano, C., Pagliusi, P., & Cipparrone, G. (2006). *Appl. Phys. Lett.*, *89*, 121105.
[12] Nersisyan, S. R., Tabiryan, N. V., Steeves, D. M., & Kimbal, B. R. (2009). *J. Nonlinear. Opt. Phys. Mater.*, *18*, 1–47.
[13] Eakin, J., Xie, Y., Pelcovits, R., Radcliffe, M. D., & Crawford, G. P. (2004). *App. Phys. Lett.*, *85*, 1671–1673.
[14] Crawford, G. P., Eakin, J., Radcliffe, M. D., Callan-Jones A., & Pelcovits, R. (2005). *J. Appl. Phys.*, *98*, 123102.
[15] Chigrinov, V., Prudnikova, E., Kozenkov, V., Kwok, H., Akiyama, H., Kawara, T., Takada, H., & Takatsu, H. (2002). *Liq. Cryst.*, *29*, 1321–1327.
[16] Yaroshchuk, O., Ho, J., Chigrinov, V., & Kwok, H. S. (2007). *Jpn. J. Appl. Phys.*, *46*, 2995–2998.

[17] Sarkissian, H., Tabirian, N., Park, B., & Zeldovich, B. (2006). *Mol. Cryst. Liq. Cryst.*, *451*, 1–19.
[18] Provenzano, C., Pagliusi, P., & Cipparrone, G. (2006). *Appl. Phys. Lett.*, *89*, 121105.
[19] Escuti, M. J., Oh, C., Sànchez, C., Bastiaansen, C. W. M., & Broer, D. J. (2006). *Proc. SPIE*, *6302*, 630207.
[20] Nersisyan, S. R., Tabiryan, N. V., Steeses, D. M., Kimball, B. R., Chigrinov, V. G., & Kwok, H. S. (2010). *Appl. Opt.*, *49*, 1720–1727.
[21] Holme, N. C. R., Nikolova, L., Ramanujam, P. S., & Hvilsted, S. (1997). *Appl. Phys. Lett.*, *70*, 1518–1520.
[22] Lagugné Labarthet, F., Buffeteau, T., & Sourisseau, C. (1999). *J. Phys. Chem. B*, *103*, 6690–6699.
[23] Provenzano, C., Cipparrone, G., & Mazzulla A. (2006). *Appl. Opt.*, *45*, 3929–3934.
[24] Pagliusi, P., Lepera, E., Provenzano, C., Mazzulla A., & Cipparrone, G. (2011). *Proc. SPIE*, *8069*, 806910.
[25] Provenzano, C., Pagliusi, P., Mazzulla A., & Cipparrone, G. (2010). *Opt. Lett.*, *35*, 1822–1824.